Investigation of the Process Parameters in Rotary Friction Welded Dissimilar AA7075/AA5083 Aluminum Alloy Joints on Fatigue Initiation using FEA and ANN

ANMAR MUSAID NAYIF[a], YOUNIS A. D.[b], ZIAD SHAKEEB AL SARRAF[c]
Department of Mechanical Engineering,
College of Engineering,
Mosul University,
Mosul,
IRAQ

[a]ORCiD: https://orcid.org/ 0009-0002-7965-8421
[b]ORCiD: https://orcid.org/0000-0001-5145-5716
[c]ORCiD: https://orcid.org/0000-0001-9957-4386

Abstract: - The rotary friction welding (RFW) method is one of the most widespread methods in the world for producing bimetallic components that require high mechanical strength. Simulations play a vital role in improving energy efficiency and reducing environmental impact, aligning with the sustainability goals of modern industry. A neural network (NN)-based incremental learning system was developed to predict crack growth and fatigue for AA5083 and AA7075 aluminum alloys. The results indicate the ability of this method to accommodate the input temperatures and the S-N curve and provide reliable predictions of expected fatigue. This method can reduce labor costs and time spent on crack propagation tests, enhancing the effectiveness of production processes and reducing process costs. This work also reveals the ability of neural . It maynetworks (NN) in monotonic function extrapolation like the S-N curve, which may pave the way for a wide variety of monotonic function-predicting problems. In future studies, a neural network (NN)-based increment learning scheme could be trained with random parts of individual S–N curves and applied to predict the rest. Additionally, the verification utilizing AISI 2205 and AISI 1020 steel has observed that neural networks may obtain S-N curve values for another metal with less than an 8% error rate. Friction pressure increases temperature, deformation, and stress in welding processes. Friction pressure 17 MPa increases temperature to 355 degrees Celsius, while Friction pressure 23 MPa increases deformation to 0.020 mm. A friction pressure of 29 MPa increases equivalent stress to 110 MPa. The indication of the S-N curve shows that increasing welding pressure increases Alternating Stress. Friction pressure also increases life, with minimum life cycles reaching 171040 cycles at 17 MPa, 195560 cycles at 23 MPa, and 283690 cycles at 29 MPa. Comparing research and simulation results, convergence is less than 8%, reducing error.

Key-Words: - Rotary friction welding, Fatigue, Artificial neural network (ANN), number of cycles to failure, S-N Curve, Equivalent stress.

Received: April 3, 2024. Revised: August 11, 2024. Accepted: September 13, 2024. Published: October 31, 2024.

1 Introduction

Modeling and simulation are crucial in the engineering sector for understanding complex phenomena and improving designs and processes. Fatigue fractures in welded shafts, particularly those formed by Rotary Friction Welding (RFW), are a significant issue in sectors like aerospace, automotive, and oil & gas. Understanding and forecasting the behavior of fatigue fractures in RFW-produced welded shafts is difficult due to the complex interaction of material characteristics, welding settings, and loading circumstances. Computer models can help engineers and academics construct insights into the physical processes involved in RFW and fatigue fracture formation and propagation, enabling the design of methods for mitigating and managing these fractures. A multidisciplinary approach is essential to address fatigue fractures in welded shafts. [1], ANSYS was used to simulate rotary friction welding processes for Al-alloy, dissimilar, and composite materials. A mathematical model was developed to characterize heat transport, frictional force, and plastic deformation heat production. Results showed that

increasing welding parameters increased welding temperature and axial shortening, with satisfactory agreement with experimental investigations. The study, [2], investigates the mechanical properties of uniting Austenitic stainless steel AISI304 and Low-carbon steel ST-37 using rotary friction welding techniques. Results show perfect welding settings with acceptable characteristics, with a highest tensile strength of 596.3 MPa at 1030 RPM, [3]. The study explores the impact of torque modulation on rotary friction welding, a process that has been around since WWII. It reveals that energy inputs can cause changes in weld microstructure and suggests potential improvements. [4], friction welding, a non-traditional technique, primarily focuses on Rotary Friction Welding (RFW), which converts kinetic energy into thermal energy, resulting in high-quality welds and high-efficiency coefficients. [5], the role of deep learning in improving the performance of shallow or conventional neural networks—specifically, Back Propagation Neural Networks—has been studied (BPNN). The majority of the research presented in this paper concentrated on employing deep ANN to fulfill the recognition procedure. The accuracy and cost function reduction with lost values between what we already have from defined instances or scenarios in the database is the basis for comparing the suggested system with other studies. [6], he study examined the thermal behavior of AA6351 T6 aluminum and AISI 304L stainless steel connections during friction welding using a thermocouple system. Results revealed temperature distribution at the bonding interface affects gradients, dissipation, heating rates, cooling, and maximum temperatures. The study, [7], examined the impact of process parameters on the mechanical properties of SS304 austenitic stainless steel and SS430 ferritic steel cylindrical rods through friction welding, revealing high tensile strength. [8], an attempt has been successfully made to develop a model to predict the effect of input parameters on weld bead geometry of submerged arc welding (SAW) process with the help of neural network technique and analysis of various process control variables and the important of weld bead parameters in submerged arc welding. The study, [9], connected AISI 4140 and AISI 1050 steel, reducing raw material costs. It examined mechanical characteristics, structural investigations, joint strength verification, and optimal welding settings, achieving 6% greater tensile strength. The study, [10], examines friction welding techniques for forming an aluminum matrix composite with SiCp particles, utilizing optical and electron microscopy, lap shear strength tests, and microhardness measurements.

2 Method Statement

2.1 Materials

The AA5083 and AA7075 aluminum alloy rods that were employed in this investigation were treated with H112 and T6, respectively. Table 1 gives their chemical compositions, and Figure 1 depicts the microstructures of the two base metals, [11].

According to Figure 1(a), the AA7075's microstructure is made up of elongated grains that run parallel to the direction of rolling which is typical of wrought products. Similar microstructural characteristics are seen in AA5083 in Figure 1(b), although in contrast to AA7075, AA5083's microstructure shows coarser grains. Table 2 displays the mechanical characteristics of base metals AA7075 and AA5083 as determined by measurements with the standards for each metal indicated in brackets. To ensure consistency, the tensile tests were carried out in triplicate using tensile specimens that complied with ASTM E8/E8M-16 standards. On the cross-section of the rods, measurements of hardness were made along the radial direction and the center line of the parallel section of the rods. Concerning Table 2, it is clear that AA7075 has more strength and hardness than AA5083, [11].

Table 1. Chemical compositions of AA5083 and AA7075 (wt. %), [11]

Material	Mg	Zn	Mn	Fe	Cr	Si	Cu	Ti	Al
AA5083	4.45	0.03	0.45	0.19	0.07	0.08	0.02	0.01	Bal.
AA7075	2.25	5.21	0.12	0.25	0.21	0.32	1.31	0.09	Bal.

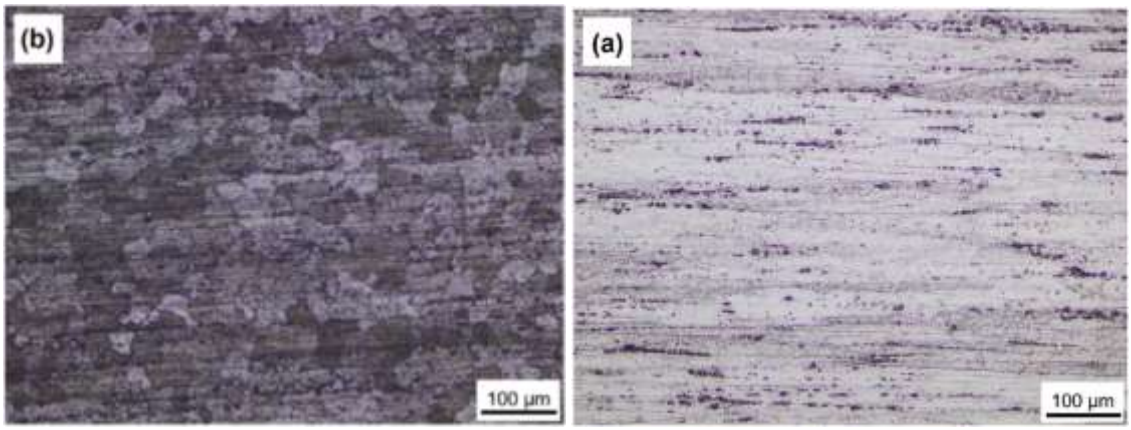

Fig. 1: Microstructures of aluminum alloy rods: (a) AA7075 and (b) AA5083, [1]

Table 2. Mechanical properties of the base materials, [12]

Mechanical Properties	AA5083	AA7075
Tensile strength (MPa)	$294.9 \pm 05.4(282\ \text{min})$	$592.6 \pm 7.4(556\ \text{min})$
Yield strength (MPa)	$176.6 \pm 14.9(171\ \text{min})$	$414.8 \pm 5.3(495\ \text{min})$
Ductility (% elongation)	$25.7 \pm 0.89(27.5)$	$9.6 \pm 0.3(10)$
Vickers microhardness (Hv)	$86.4 \pm 3.77(96)$	$185.6 \pm 8.4(175)$

2.2 The Rotary Friction Welding Process

In this project, a lathe machine was modified to create a rotating friction welding machine. The samples were created using a milling machine in the shape of a 50 mm long, 15 mm diameter cylindrical rod, [11]. As indicated in Figure 2, the second rod, AA7075, served as the rotating side (RS), and the cylindrical rod AA5083 was positioned as the stationary side (SS) that was moved axially.


Fig. 2: Design rod

The RFW procedures as shown in Figure 3 were used to perform RFW processes on the dissimilar AA7075/AA5083 aluminum alloys. As soon as the moving surface contacted the stationary surface, the welding process's first step began. This step is denoted by A in Figure 3 and involved a rapid increase in axial pressure from 0 to 17,23,29 MPa for two seconds. Step B then involved friction at a constant pressure of 17, 23, and 29 MPa for ten seconds. The production of bonds was triggered by the interruption of the rotational speed at the end of the friction stage (step C) and the application of an upset pressure 115 MPa for 4 s (step D). Welding heat cycles as well as variations in burn-off length as the response parameter were noted.

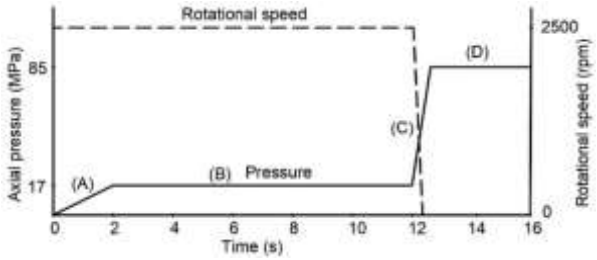

Fig. 3: Rotary friction welding process stages, [11]

2.3 Artificial Neural Network (ANN)

Neural network-based methods are of great learning and generalization ability. Where the temperatures that were extracted from the simulation of the welding process were entered and entered into the artificial intelligence program to obtain the values of the s-n curve. As seen in Figure 5. So enormous success has been achieved in many industry applications, [11]. NN-based methods were introduced to fatigue and fracture research areas in different topics such as S–N curves determination [12], stress intensity factor prediction, the useful life prediction Particularly, more and more NN-based methods have shown their capabilities and effectiveness in fatigue–crack growth rate prediction. The neural network trained to simulate the crack growth rate of aluminum alloy prediction is in good agreement with the experimental data with an error of less than 8 %, [13].

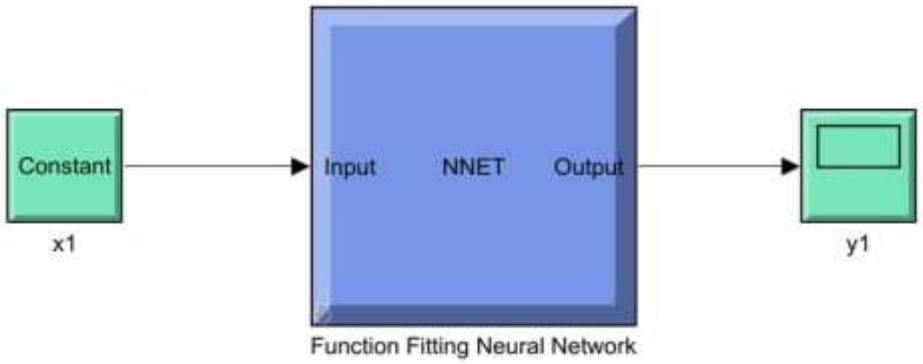

Fig. 4: ANN diagram, [12]

2.4 Methodology

Generally, unstructured matrices are effective for complex calculations, so for the above reason, the unstructured tetrahedron frameworks were utilized in the ongoing review. With just one phase from the user, ANSYS can generate solid geometry meshes and three-dimensional models. In this investigation, there were cells extracted from a total of (1208270) tetrahedron elements, and the sizing of each element was 0.5mm see Figure 4.

An accurate network must be created to solve the equations because the simulation process depends on complicated algorithms to work on the matrices present in the domain. After that, use the mesh's dependability to find a remedy and bring the outcomes to a stable condition. It is important to create more than one network and mesh dependability due to the variety of models that have been simulated. The value of the element was 1208270 when the max temperature reached 422.9 C as in Table 3.

The fatigue simulation model was designed according to the dimensions mentioned in Figure 6. This sample resulted from the simulation of rotary friction welding, where the length of the sample was 90 mm and its diameter was 12 mm.

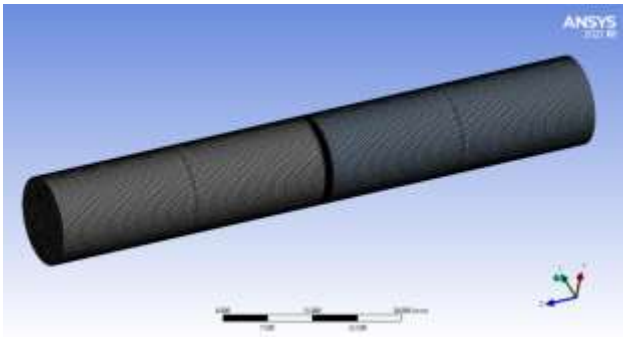

Fig. 5: Mesh generated

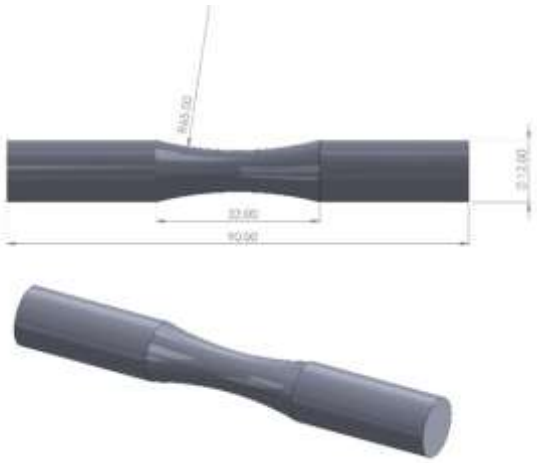

Fig. 6: Fatigue Cracks domain

Table 3. Mesh independency

Case	Element	node	Max temperature C
1	694473	138678	174.82
2	845695	326866	171.90
3	056566	524326	170.74
4	208270	701776	170.67

Where the process of stabilizing the sample was carried out on one hand, and a pressure of 20 tons was used to obtain the fatigue state in the sample during the simulation process. The fatigue analysis in ANSYS Workbench estimates the number of cycles to failure using a variety of fatigue life estimation techniques, including the Stress-Life (S-N) and Strain-Life (-N) approaches. The specific material qualities, loading conditions, and method selected all affect the equations that are utilized for fatigue analysis. The equation used to calculate the fatigue life (N) for a Stress-Life (S-N) approach in ANSYS, which is frequently utilized for metals, is frequently represented as [14]:

$$N=(A/(\sigma)^{\wedge}\Lambda\ m)+(B/(\sigma)^{\wedge}\Lambda\ n) \quad (1)$$

Where: The cycle count before failure is N. The amplitude of the alternating stress is. Material-specific constants A, B, m, and n are identified by data from fatigue tests or by material characteristics. Similar equations are utilized in the Strain-Life (-N) approach, which is used for materials that display strain-based fatigue behavior, although the terms and constants may be connected to strain rather than stress.

2.5 Mathematical Model Adopted by ANSYS software

The overall equilibrium equations for linear structural static analysis are [14]:

$$[K]\{u\} = \{F\} \quad (1)$$

or

$$[K]\{u\} = \{F^a\} + \{F^r\} \quad (2)$$

where:

$[K] = \sum_{m=1}^{N} [K_e]$ = total stiffness matrix

{u} = nodal displacement vector

N = number of elements

$[K_e]$ = element stiffness matrix (described in Element Library) (may include

the element stress stiffness matrix (described in Stress Stiffening))

$\{F^r\}$ = reaction load vector

$\{F^a\}$, the total applied load vector is defined by [11]:

$$\{F^a\} = \{F^{nd}\} + \{F^{ac}\} + \sum_{m=1}^{N} (\{F_e^{th}\} + \{F_e^{pr}\}) \quad (3)$$

Where:

$\{F^{nd}\}$ = applied nodal load vector

$\{F^{ac}\} = -[M]\{a_c\} =$ Acceleration load vector

$[M] = \sum_{m=1}^{N} [M_e]$ = total mass matrix

$[M_e]$ = element mass matrix (described in Derivation of Structural Matrices)

$\{a_c\}$ = total acceleration vector (defined in Acceleration Effect)

$\{F_e^{th}\}$ = element thermal load vector (described in Derivation of Structural Matrices)

$\{F_e^{pr}\}$ =element pressure load vector (described in Derivation of Structural Matrices Consider a one-element column model that is solely loaded by its own weight to demonstrate the load vectors. Reaction Load Vectors and Applied Load Vectors Although the lower applied gravity load is applied directly to the imposed displacement and so does not create strain, it contributes just as much to the reaction load vector as the higher applied gravity load. In addition, any applied loads on a particular DOF are disregarded if the stiffness for that DOF is 0

The equation governing transient thermal behavior, also known as the heat conduction equation or the heat diffusion equation, describes how temperature changes within a solid over time due to heat conduction. This equation is a fundamental tool in thermal analysis and can be expressed as [10]:

$$\rho c \frac{\partial T}{\partial t} = \nabla \cdot (k \nabla T) + Q \quad (4)$$

Where:

ρ Is the material density $\left(\frac{\mathbf{kg}}{\mathbf{m^3}}\right)$.

c Is the specific heat capacity $\left(\frac{\mathbf{J}}{\mathbf{kg \cdot K}}\right)$.

T Is the temperature $(\mathbf{°C})$ as a function of time t and spatial coordinates.

$\frac{\partial T}{\partial t}$ Represents the rate of change of temperature with respect to time.

k Is the thermal conductivity $\left(\frac{\mathbf{W}}{\mathbf{m \cdot K}}\right)$, which characterizes how well the material conducts heat.

∇ Is the gradient operator, and $\nabla \cdot$ represents the divergence operator, used to describe heat flow.

Q Represents any internal heat generation or external heat sources $\left(\frac{\mathbf{W}}{\mathbf{m^3}}\right)$.This equation states that the change in temperature $\left(\frac{\partial T}{\partial t}\right)$ is proportional to the heat conduction term on the right side, which is the divergence of the thermal conductivity gradient, and any heat sources or sinks within the material, [15].

3 Results and Discussion

3.1 The Effect of Friction Pressure on the Temperature of the Rotary Friction Welding Process

The quality and properties of a weld are significantly influenced by friction pressure and

temperature during rotary friction welding. This solid-state welding technique involves rotating two parts against each other, applying pressure to generate frictional heat, and joining materials. The temperature profile within the welding zone is directly influenced by friction pressure and rotational speed. To achieve the ideal temperature range for efficient material softening and joining, precise control of friction pressure is necessary. Modern rotary friction welding machines often have automatic pressure control systems to maintain stable temperature conditions. Engineers and researchers study the link between friction pressure and temperature to create precise control plans and recommendations for dependable and high-quality welding across various industries, [14]. From Figure 7 (Appendix) it is evident that the Friction pressure increases the temperature generated by friction pressure, as the temperature reached 355 degrees Celsius at the Friction pressure of 17 MPa, and at the Friction pressure of 23 MPa the temperature reached 384 degrees Celsius, while at the Friction pressure, 29 MPa the temperature reached to 413 degrees Celsius. The increase in temperature with the increase in the speed of rotation of the axes in rotary friction welding is primarily due to the conversion of mechanical energy into heat through friction at the interface between the two rotating components. When the rotation speed increases, several factors contribute to the rise in temperature:

- Increased Frictional Work: Higher rotation speeds lead to greater relative motion between the materials being welded. This increased relative motion results in more significant frictional forces and work done at the interface. As the materials rub against each other with greater intensity and speed, a larger amount of mechanical energy is converted into heat, [16].
- Increased Shear Forces: The higher rotational velocity induces stronger shear forces at the interface. Shearing action between the materials generates a considerable amount of frictional heat, which further raises the temperature, [17].
- More Frequent Material Mixing: The increased speed causes more frequent and intense mixing of material at the weld interface. This mixing creates a localized temperature rise as the material is exposed to greater shearing and deformation, [18].
- Reduced Heat Dissipation: At higher rotation speeds, there is less time for heat to dissipate away from the weld zone, which allows the temperature to build up more quickly, [19].
- Plastic Deformation: The intense mechanical energy generated at higher rotation speeds causes plastic deformation of the material, making it more malleable. This plastic deformation is necessary for the materials to bond and form a strong metallurgical joint, [20].
- Increased Strain Rate: A higher rotation speed typically corresponds to a higher strain rate, which is the rate at which the material is deformed. The increased strain rate contributes to higher temperatures because it increases the rate at which work is done on the material, [21].

3.2 Deformation with Time of Rotary Friction Welding Process at Different Friction Pressure

The rotary friction welding process, also known as spin welding, involves rotating components against each other while applying pressure. The heat produced by friction softens materials, making bonding easier. The deformation properties of welded components are significantly influenced by friction pressure and other process variables. Higher friction pressure results in more substantial deformation, while lower pressure results in less deformation and longer welding sessions. Engineers and researchers must strike a balance between pressure and distortion to produce dependable welds. Different materials react differently to deformation, with some being more malleable and others more brittle.

Modern rotary friction welding equipment uses automated control systems to monitor and control deformation. Understanding friction pressure influences deformation can help develop precise control strategies for industries like automotive, aerospace, and manufacturing, [22].

From Figure 8 (Appendix) and Figure 9 it is evident that the Friction pressure increases the deformation generated by friction pressure, as the deformation reached 0.020 mm at the Friction pressure of 17 MPa, and at the Friction pressure, of 23 MPa the deformation reached 0.022 mm, while at the Friction pressure, 29 MPa the deformation reached to 0.025 mm .

- Material Behavior: AA5083, with its higher magnesium content, tends to be more ductile and exhibits good formability. This can be advantageous in friction welding, as it can deform more readily to achieve a strong weld joint. Work Hardening: AA5083 is known for its work-hardening behavior. During friction welding, it can experience significant plastic deformation and work hardening, which can contribute to a strong and durable weld. AA7075, while strong, may not deform as

readily as AA5083 and may not work harden to the same extent. This can make it more challenging to achieve a strong weld in certain friction welding applications [23], [24].

- Heat Generation: The heat generated during friction welding is critical in plastic deformation. The heat input can vary depending on the welding parameters and the material's thermal conductivity. AA7075, with its higher thermal conductivity, may dissipate heat more efficiently during the welding process, affecting the plastic deformation.

When friction welding AA5083 and AA7075, AA5083's greater ductility and work-hardening characteristics can be advantageous for achieving a strong weld. However, the success of the welding process also depends on other factors such as welding parameters, tool design, and the specific requirements of the joint, [20].

3.3 Equivalent Stress Effect Of Rotary Friction Welding Process at Different Friction Pressure

Friction pressure significantly impacts the quality, integrity, and performance of welded connections during rotary friction welding. The process involves rotating components and applying pressure to create frictional heat, causing material flow and deformation. Higher friction pressure leads to greater stress levels in the welding zone. Residual tensions may form as the welded connection cools down. The strength and dependability of a welded connection depend on the level and distribution of stress within the joint. To ensure stress concentration remains within permissible limits, friction pressure must be properly controlled. Modern rotary friction welding equipment often includes advanced control and monitoring systems to control friction pressure, resulting in reliable, highly strengthened joints with controlled stress levels. Understanding friction pressure's impact on stress can lead to precise management techniques and standards for strong and durable welds in sectors like automotive, aerospace, and manufacturing.

From Figure 10 (Appendix) and Figure 11 (Appendix) it is evident that the Friction pressure increases the Stress generated by friction pressure, as the Stress reached 110 MPa at the Friction pressure of 17 MPa, and at the Friction pressure, of 23 MPa the Stress reached 136 MPa, while at the Friction pressure, 29 MPa the Stress reached to 154 MPa.

When the friction pressure is increased in rotary friction welding, it generally implies that more force is applied to the interface of the materials being welded. This increased force leads to greater frictional heating at the interface, which in turn affects the material properties and generates additional stress. Higher friction pressure results in greater frictional forces at the interface between the two materials. This can lead to increased plastic deformation and thermal effects, contributing to higher equivalent stresses. The response of materials to heat and pressure can vary, affecting how they deform and experience stress during the welding process. Different materials have different thermal and mechanical properties that influence equivalent stress. It's important to note that while increasing friction pressure may enhance the welding process by promoting better material bonding, there is a limit to the pressure that can be applied without causing adverse effects such as material degradation, excessive plastic deformation, or other undesirable outcomes, [23].

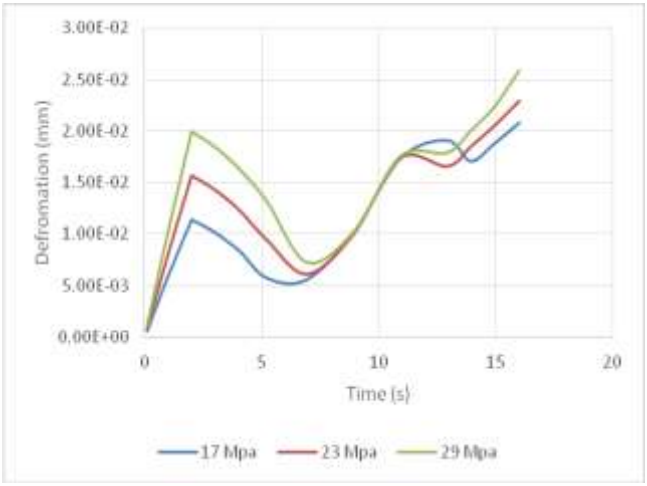

Fig. 9: Deformation with time of rotary friction welding process at different Friction pressure

3.4 Alternating Stress with the Number of Cycles to Failure for Different Welding Pressure

Through the temperatures obtained by varying the friction pressure and entering the results into the artificial intelligence program. S-N curve diagrams were obtained for all cases; Figure 12 (Appendix) shows that the increase in welding pressure increases the amount of Alternating Stress.

Figure 13 (Appendix), it is evident that the Friction pressure increases the Life generated by Friction pressure, as the minimum life reached 171040 cycles at a Friction pressure of 17 MPa, and

at the Friction pressure, of 23 MPa the minimum life reached 195560 cycles, while at the Friction pressure, 29 MPa the minimum life reached 283690 cycles.

4 ANN Validation for Rotary Friction Welding of AISI 2205 and AISI 1020

Commercially available 12 mm x 6000 mm bars of AISI 1020 low carbon steel and AISI 2205 duplex stainless steel were employed as the materials for the experimental experiments. To get rid of any pollution, rust, and oxide coatings on the butt surface, the materials were cut at a strip sawing machine at a length of 72 mm, and the specimens were turned at a turning lathe at a diameter of 70 mm, [24]. The steel couples' chemical makeup, as determined by the samples they served as Each specimen underwent tensile and fatigue testing to determine the effects of the welding parameters on the bond strength and the degrading processes. The outcome of the test specimens' tensile strength measurements. The tests indicated that the maximum tensile stresses for the AISI 1020 steel and the AISI 2205 duplex stainless steel employed in them were 610,780.

Where the comparison was made with the research and obtaining information and applying it to the simulation process, where it was found that the convergence reaches less than 8%, the percentage of error between the two works, as in Figure 14 (Appendix).

5 Conclusion

In this study, rotary friction welding was used to connect the aluminum alloy couples AA5083 and AA7075, which had different chemical compositions and different manufacturing parameters. When the friction pressure is increased in rotary friction welding, it generally implies that more force is applied to the interface of the materials that are being welded. This increased force leads to greater frictional heating at the interface, which in turn affects the material properties and generates additional stress. Higher friction pressure results in greater frictional forces at the interface between the two materials. This can lead to increased plastic deformation and thermal effects, contributing to higher equivalent stresses. Therefore, the equivalent stress results show an increase in Friction pressure. The increase in welding pressure increases the amount of Alternating Stress. Increased pressure can enhance the mixing of material at the weld interface, reducing the presence of distinct zones with different properties. Homogeneous mixing contributes to a more uniform stress distribution, improving the overall fatigue performance. It's important to note that while higher welding pressure can generally improve fatigue performance, there is an optimal range for pressure, and excessive pressure may lead to other issues, such as material damage or distortion. The specific effects of welding parameters can vary depending on the alloy and the welding process used, so careful optimization is required for each application. Additionally, the fatigue behavior is influenced by factors like the applied load spectrum, environmental conditions, and post-weld treatments. Also, the validation by using AISI 1020 steel and the AISI 2205 It has been noted that it is possible to use neural networks to obtain S-N curve values for other metals with an error rate of less than 8%.

Declaration of Generative AI and AI-assisted Technologies in the Writing Process

The authors declared that the language of this current work was carried out based on using AI and their AI-Assisted technologies, in writing parts of sentences through using these technologies in order to improve the readability and language in academic manner.

References:

[1] F. I. Salih, A. S. Dawood, and A. A. Hamid, "Review on the Thermal Characterizations of Rotary Friction Welding," *Al-Rafidain Engineering Journal (AREJ)*, vol. 27, no. 1, Art. no. 1, Mar. 2022, doi: 10.33899/rengj.2021.132049.1141.

[2] S. Alghazalah and S. Ali, "Effect of Forging Pressure on Mechanical Properties of Two Dissimilar Welded Joints of Austenitic Stainless Steel AISI304 and Low Carbon Steel ST-37 Using Rotary Friction Welding Techniques," *Universal Journal of Mechanical Engineering*, vol. 11, pp. 1–12, Mar. 2023, doi: 10.13189/ujme.2023.110101.

[3] R. C. Ashwell, "*Manufacturing modification through process manipulation in inertia friction welding: enhanced functionality rotary friction welding,"* d_en, University of Birmingham, 2021, [Online]. https://etheses.bham.ac.uk/id/eprint/11451/ (Accessed Date: March 18, 2024)

[4] N. Shete and S. Deokar, "A Review Paper on Rotary Friction Welding," vol. 5, pp. 1557–1560, Jun. 2017.

[5] E. Alves, R. C. Toledo, F. P. Neto, F. G. Botter, and C. Y. An, "Experimental Thermal Analysis in Rotary Friction Welding of Dissimilar Materials," *Journal of Aerospace Technology and Management*, vol. 11, Sep. 2019. [Online]. https://jatm.com.br/jatm/article/view/1068 (Accessed Date: October 12, 2024).

[6] O. M. Abduljawad, "Enhancing Drivers' Attention By A Smart Binary Matching Machine to Avoid Accidents," *Al-Rafidain Engineering Journal (AREJ)*, vol. 28, no. 2, Art. no. 2, Sep. 2023, doi: 10.33899/rengj.2023.138781.1240.

[7] P. Anitha, M. ChandraMajumder, S. Veerasamy, and R. Selvarajan, "Investigation of Mechanical Properties of Friction-welded AISI 304 with AISI 430 Dissimilar Steels," *Materials Physics and Chemistry*, vol. 1, p. 8, May 2019, doi:

[8] E. P. Alves, F. Piorino Neto, and C. Y. An, "Welding of AA1050 aluminum with AISI 304 stainless steel by rotary friction welding process," *J. Aerosp. Technol. Manag.*, vol. 2, pp. 301–306, Dec. 2010, doi: 10.5028/jatm.2010.02037110.

[9] M. Saeed and Z. Sarraf, "Using Artificial Neural Networks to Predict the Effect of Input Parameters on Weld Bead Geometry for SAW Process," *Journal Européen des Systèmes Automatisés*, vol. 54, pp. 309–315, Apr. 2021, doi: 10.18280/jesa.540213.

[10] N. Özdemir and Z. Balaban, "Friction welding of Al-Cu-SiC composite to AISI 304 austenitic stainless steel," *IJIEA*, vol. 1, no. 1, Art. no. 1, Jun. 2017.

[11] Metals, Free Full-Text | Effect of Rotational Speed on Static and Fatigue Properties of Rotary Friction Welded Dissimilar AA7075/AA5083 Aluminium Alloy Joints." https://doi.org/10.3390/met12010099.

[12] Artymiak P, Bukowski L, Feliks J, Narberhaus S, Zenner H. Determination of S–N curves with the application of artificial neural networks. *Fatigue Fract Eng Mater Struct*, 1999;22(8):723–8, https://doi.org/10.1046/j.1460-2695.1999.t01-1-00198.x.

[13] X. Ma, X. He, and Z. C. Tu, "Prediction of fatigue–crack growth with neural network-based increment learning scheme," *Engineering Fracture Mechanics*, vol. 241, p. 107402, Jan. 2021, doi: 10.1016/j.engfracmech.2020.107402.

[14] Ansys, Engineering Simulation Software, [Online]. https://www.ansys.com/ (Accessed Date: October 12, 2024).

[15] F. Khalfallah, Z. Boumerzoug, R. Selvarajan, and E. Raouache, "Optimization by RSM on rotary friction welding of AA1100 aluminum alloy and mild steel," *International Review of Applied Sciences and Engineering*, vol. 11, Apr. 2020, doi: 10.1556/1848.2020.00005.

[16] Calculating the energy required to undergo the conditioning phase of a titanium alloy inertia friction weld," *Journal of Manufacturing Processes*, vol. 24, pp. 186–194, Oct. 2016, doi: 10.1016/j.jmapro.2016.09.008.

[17] Z. Zhao, W. Song, Y. Jin, and J. Lu, "Effect of Rotational Speed Variation on the Flow Characteristics in the Rotor-Stator System Cavity," *Applied Sciences*, vol. 11, no. 22, Art. no. 22, Jan. 2021, doi: 10.3390/app112211000.

[18] G. Di Bella, F. Favaloro, and C. Borsellino, "Effect of Process Parameters on Friction Stir Welded Joints between Dissimilar Aluminum Alloys: A Review," *Metals*, vol. 13, no. 7, Art. no. 7, Jul. 2023, doi: 10.3390/met13071176.

[19] A. Azhagar and K. Hayakawa, "Effects of Tool Surface Geometry on Temperature Distribution and Material Properties of an Aluminum Alloy in Friction Stir Welding," *Materials Transactions*, vol. 61, no. 2, Art. no. 2, 2020, doi: 10.2320/matertrans.MT-ML2019017.

[20] K. Mori, N. Bay, L. Fratini, F. Micari, and A. E. Tekkaya, "Joining by plastic deformation," *CIRP Annals*, vol. 62, no. 2, Art. no. 2, Jan. 2013, doi: 10.1016/j.cirp.2013.05.004.

[21] B. Dalai, M. A. Moretti, P. Åkerström, V. A. Esin, and L.-E. Lindgren, "Mechanical behavior and microstructure evolution during high strain rate deformation of AA7075-T651," *SN Appl. Sci.*, vol. 4, no. 10, Art. no. 10, Sep. 2022, doi: 10.1007/s42452-022-05141-6.

[22] Aluminium Alloys, Aluminium 5083 Properties, Fabrication and Applications," AZoM.com, [Online]. https://www.azom.com/article.aspx?ArticleID=2804 (Accessed Date: Oct. 26, 2024).

[23] Senthil Murugan S., Noorul Haq A & Sathiya P., "Effect of welding parameters on the microstructure and mechanical properties of the friction-welded dissimilar joints of

AA6063 alloy and faying surface-tapered AISI304L alloy, SpringerLink." https://doi.org/10.1007/s40194-020-00846-x.

[24] S. Mercan, S. Aydin, and N. Özdemir, "Effect of welding parameters on the fatigue properties of dissimilar AISI 2205–AISI 1020 joined by friction welding," *International Journal of Fatigue*, vol. 81, pp. 78–90, Dec. 2015, doi: 10.1016/j.ijfatigue.2015.07.023.

Contribution of Individual Authors to the Creation of a Scientific Article (Ghostwriting Policy)

The authors equally contributed in the present research, at all stages from the formulation of the problem to the final findings and solution.

Sources of Funding for Research Presented in a Scientific Article or Scientific Article Itself

No funding was received for conducting this study.

Conflict of Interest

The authors have no conflicts of interest to declare .

APPENDIX

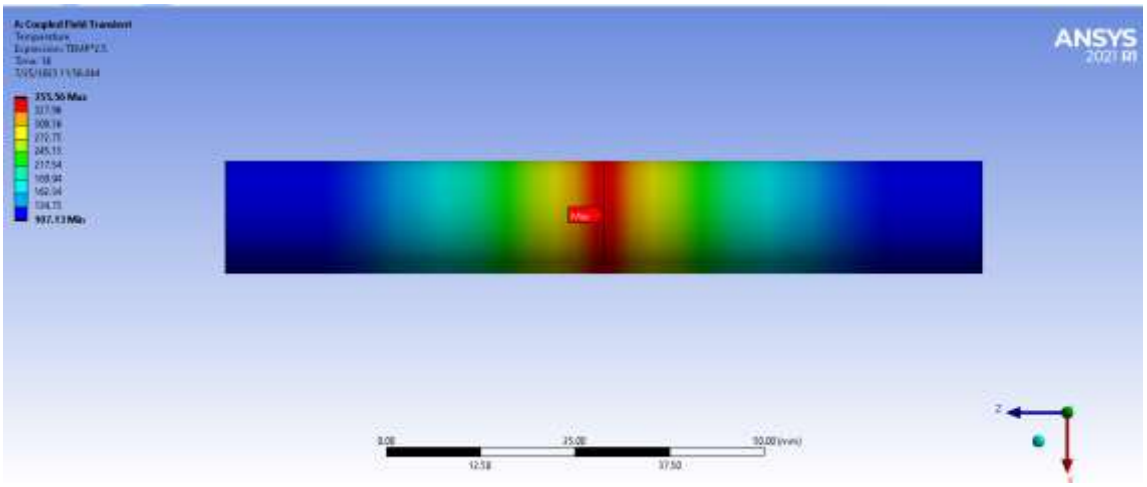

(a)

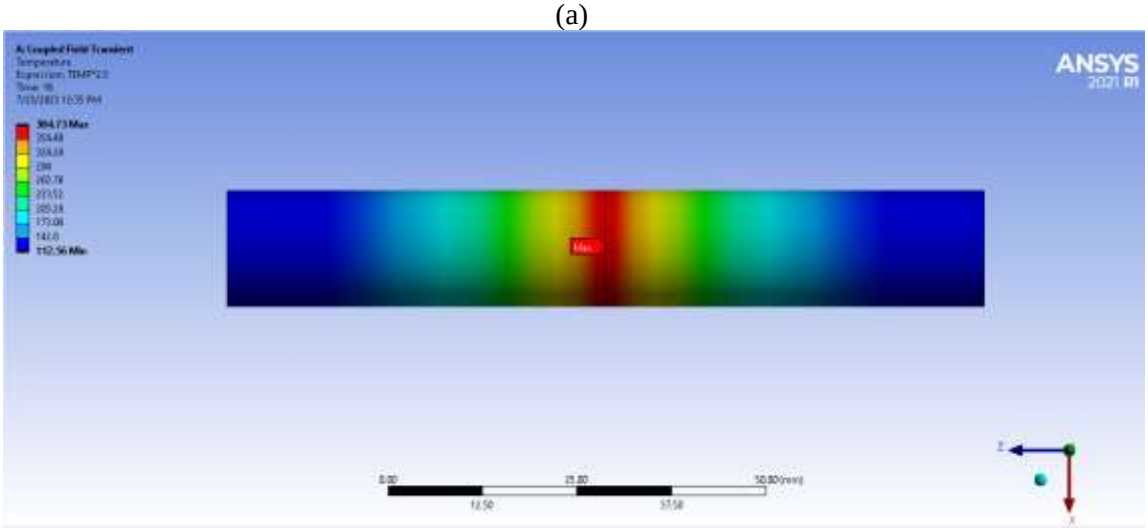

(b)

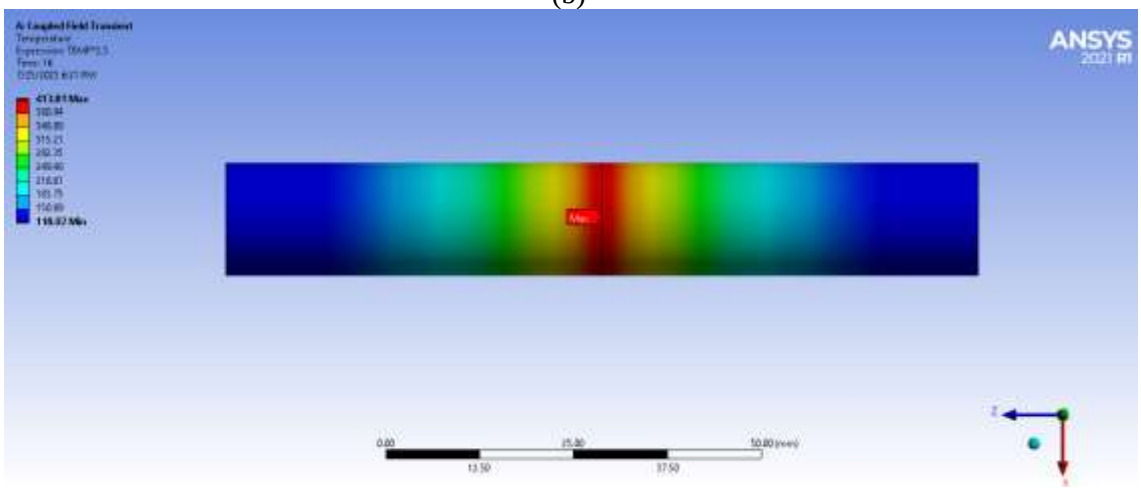

(c)

Fig. 7: Temperature contour of rotary friction welding process at different Friction pressure: (a) 17 MPa, (b) 23 MPa, (c) 29 MPa

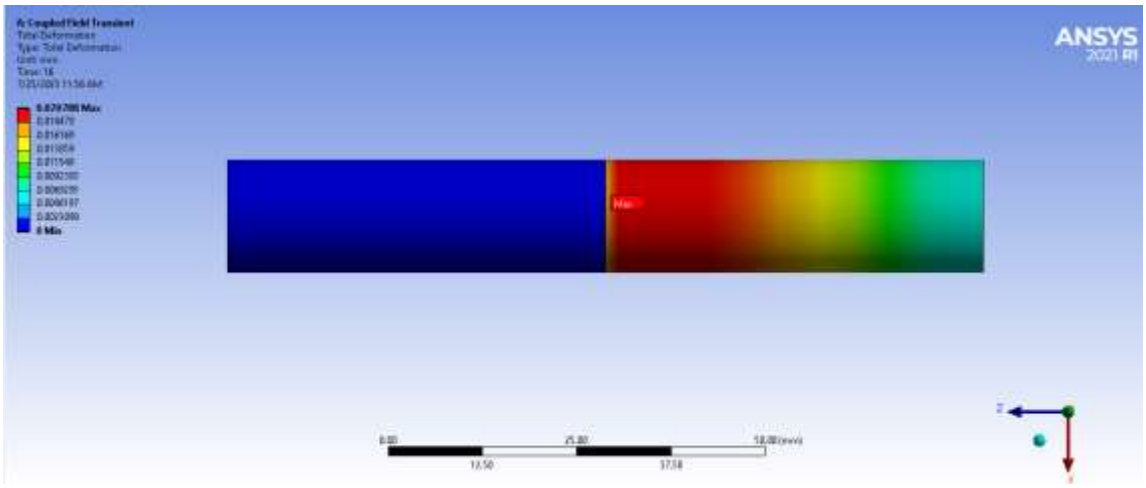

(a)

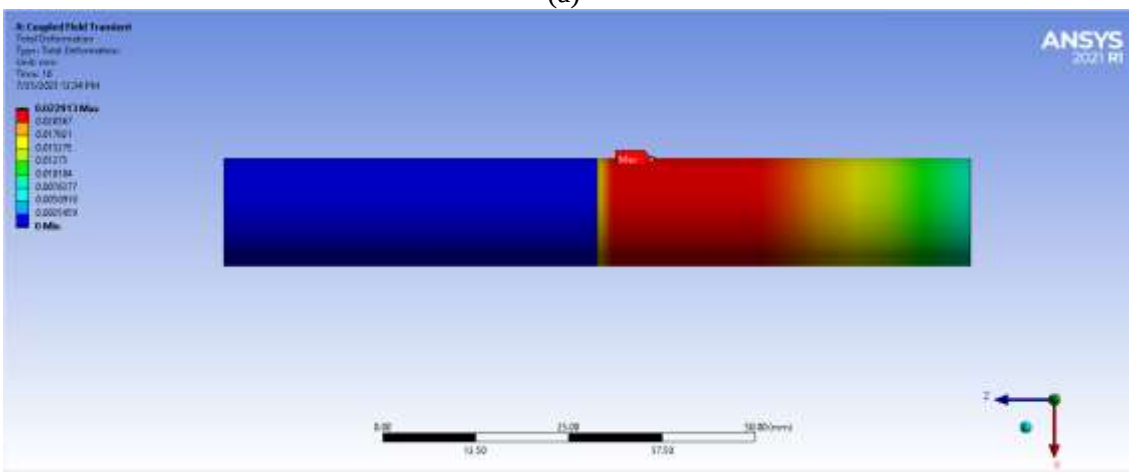

(b)

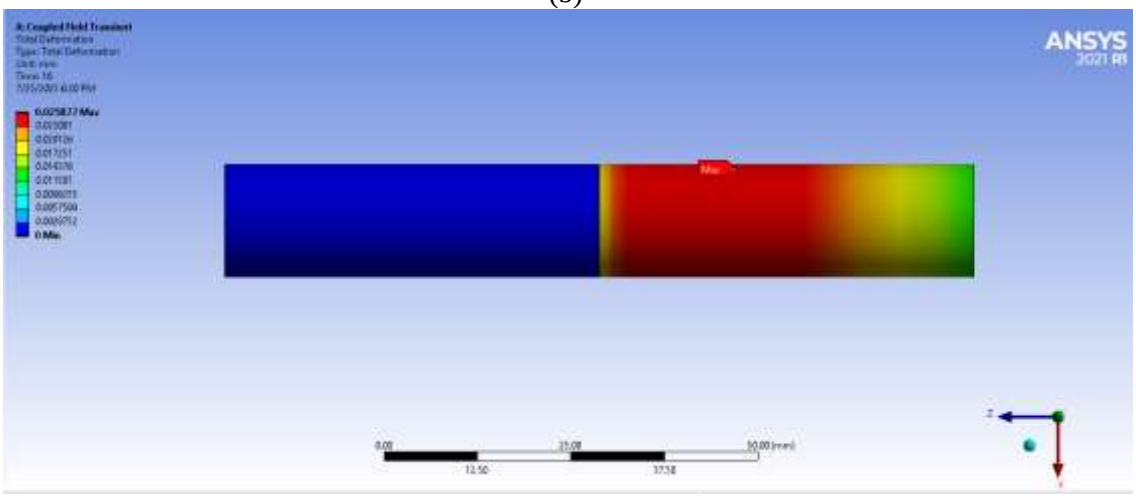

(c)

Fig. 8: Deformation contour of rotary friction welding process at different Friction pressures: (a) 17 MPa, (b) 23 MPa, (c) 29 MPa

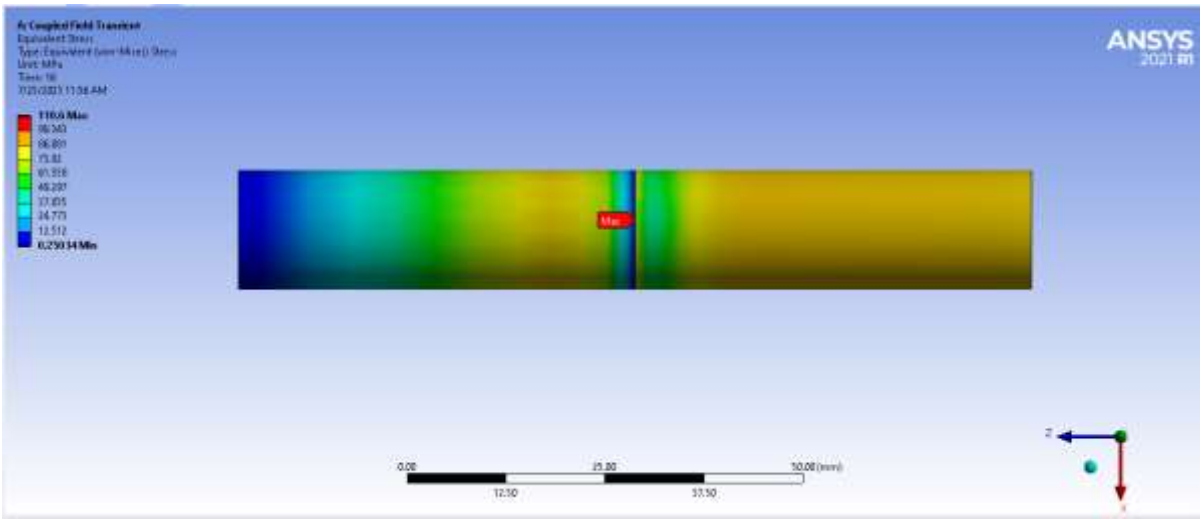

(a)

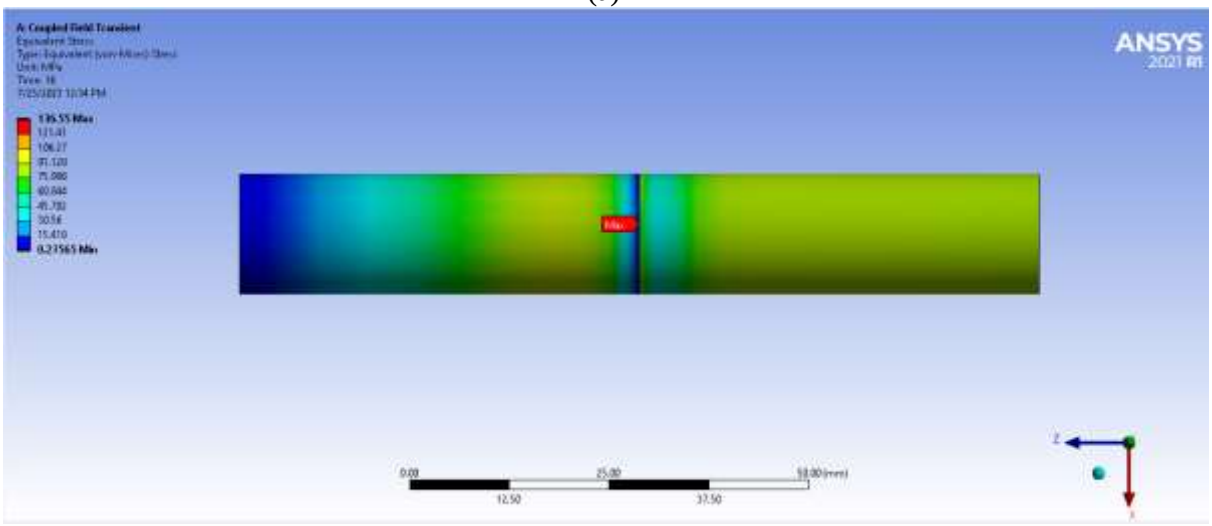

(b)

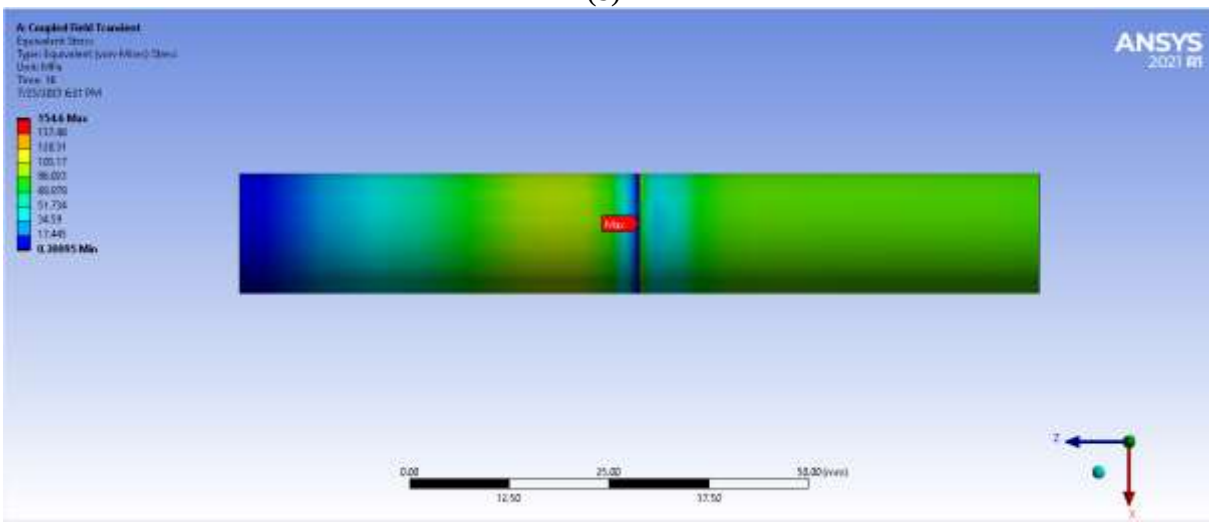

(c)

Fig. 10: Equivalent stress contour of rotary friction welding process at different Friction pressure: (a) 17 MPa, (b) 23 MPa, (c) 29 MPa

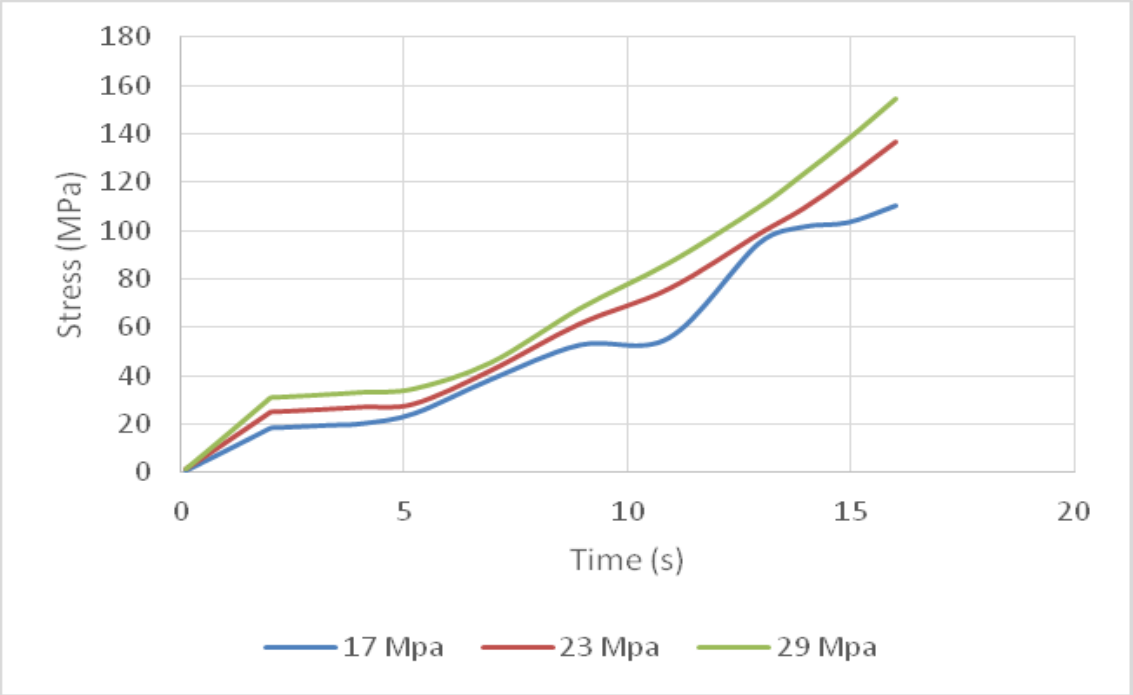

Fig. 11: Equivalent stress with time of rotary friction welding process at different Friction pressure

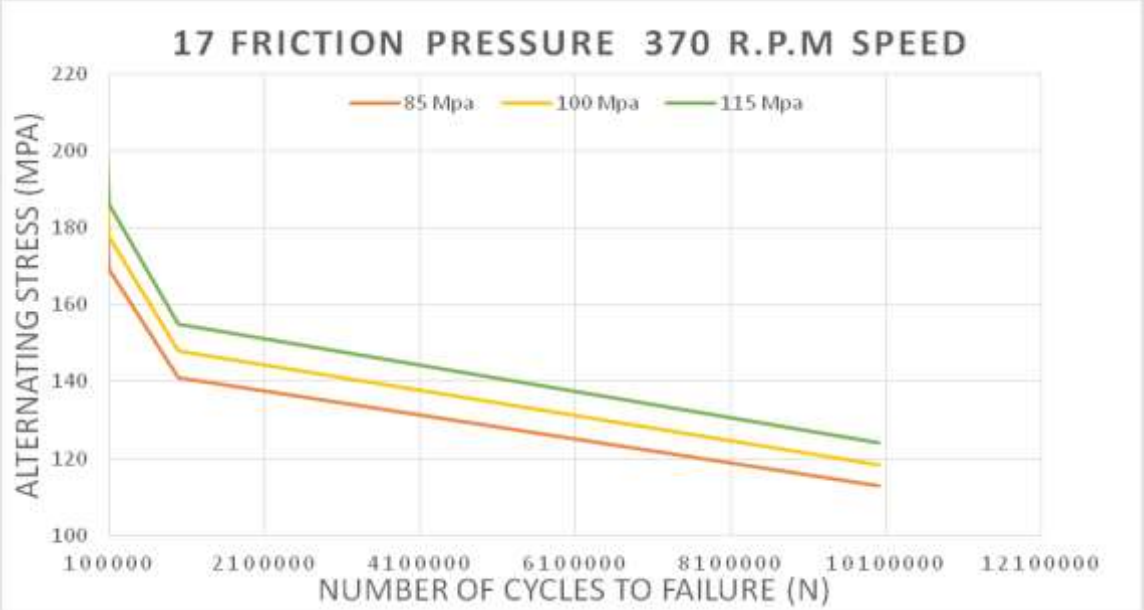

Fig. 12: Alternating Stress with Number of cycles to failure for different welding pressure

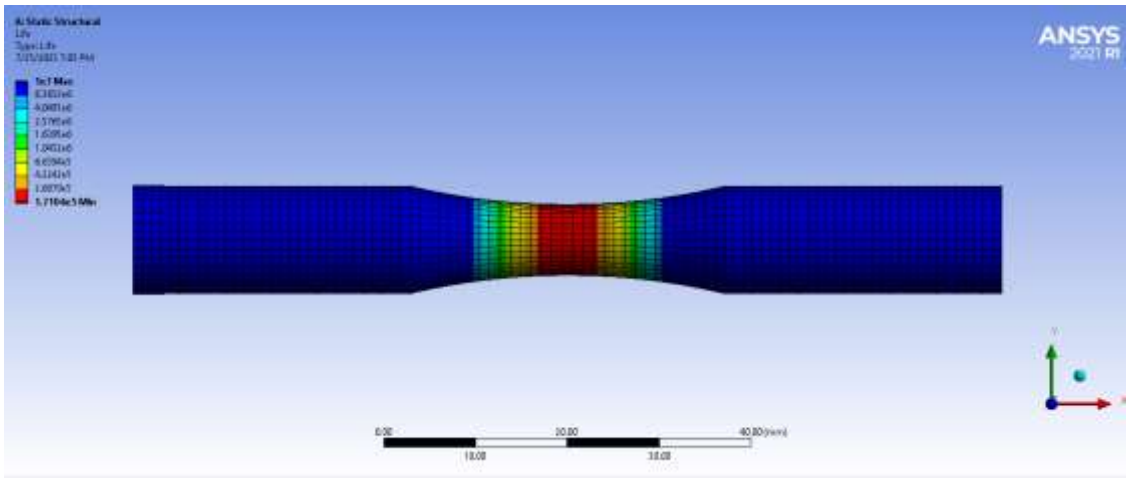

(a)

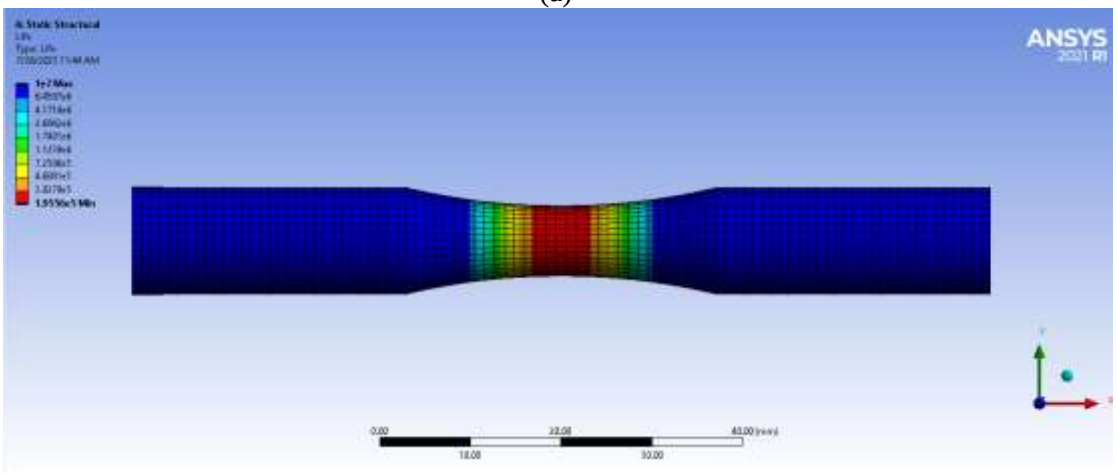

(b)

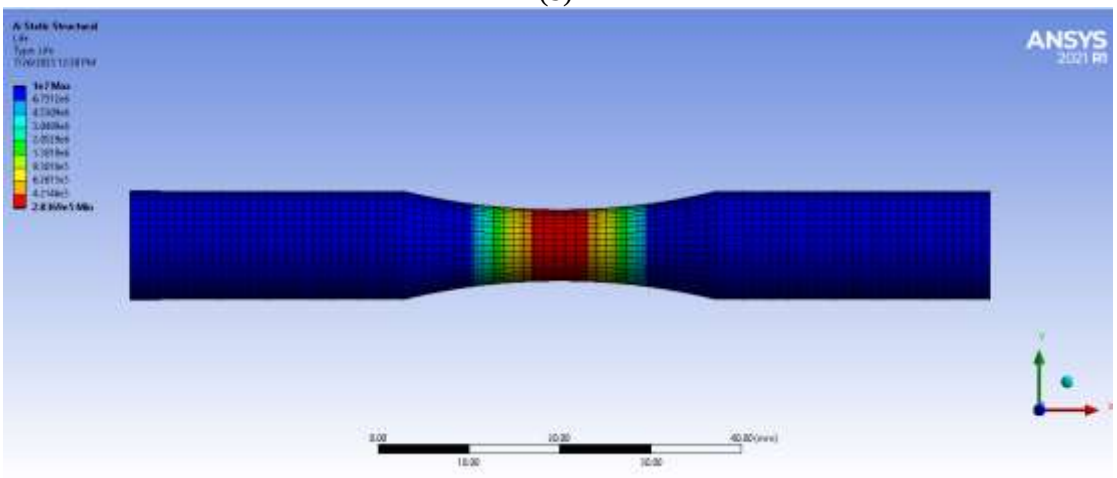

(c)

Fig. 13: Life contour of fatigue process at different Friction pressure:
(a) 17 MPa, (b) 23 MPa, (c) 29 Mpa

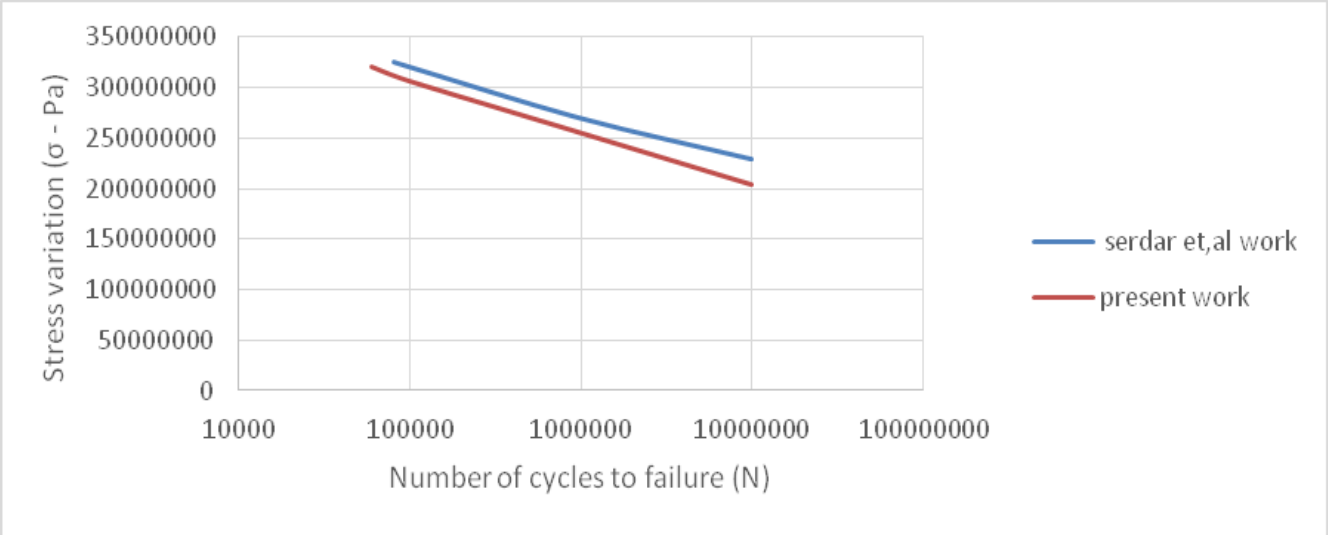

Fig. 14: Stress variation with the number of cycles to failure